ACS NANO
Cite This: ACS Nano 2018, 12, 9484–9494
www.acsnano.org

ARTICLE

Cation-Activated Avidity for Rapid Reconfiguration of DNA Nanodevices

Alexander E. Marras,[†] Ze Shi,[∥] Michael G. Lindell, III,[‡] Randy A. Patton,[†] Chao-Min Huang,[†] Lifeng Zhou,[†] Hai-Jun Su,[†] Gaurav Arya,[*,⊥] and Carlos E. Castro[*,†,§]

[†]Department of Mechanical and Aerospace Engineering, [‡]Department of Chemical and Biomolecular Engineering, and [§]Biophysics Graduate Program, The Ohio State University, Columbus, Ohio 43210, United States

[∥]Department of NanoEngineering, University of California San Diego, La Jolla, California 92093, United States

[⊥]Department of Mechanical Engineering and Materials Science, Duke University, Durham, North Carolina 27708, United States

Supporting Information

ABSTRACT: The ability to design and control DNA nanodevices with programmed conformational changes has established a foundation for molecular-scale robotics with applications in nanomanufacturing, drug delivery, and controlling enzymatic reactions. The most commonly used approach for actuating these devices, DNA binding and strand displacement, allows devices to respond to molecules in solution, but this approach is limited to response times of minutes or greater. Recent advances have enabled electrical and magnetic control of DNA structures with sub-second response times, but these methods utilize external components with additional fabrication requirements. Here, we present a simple and broadly applicable actuation method based on the avidity of many weak base-pairing interactions that respond to changes in local ionic conditions to drive large-scale conformational transitions in devices on sub-second time scales. To demonstrate such ion-mediated actuation, we modified a DNA origami hinge with short, weakly complementary single-stranded DNA overhangs, whose hybridization is sensitive to cation concentrations in solution. We triggered conformational changes with several different types of ions including mono-, di-, and trivalent ions and also illustrated the ability to engineer the actuation response with design parameters such as number and length of DNA overhangs and hinge torsional stiffness. We developed a statistical mechanical model that agrees with experimental data, enabling effective interpretation and future design of ion-induced actuation. Single-molecule Förster resonance energy-transfer measurements revealed that closing and opening transitions occur on the millisecond time scale, and these transitions can be repeated with time resolution on the scale of one second. Our results advance capabilities for rapid control of DNA nanodevices, expand the range of triggering mechanisms, and demonstrate DNA nanomachines with tunable analog responses to the local environment.

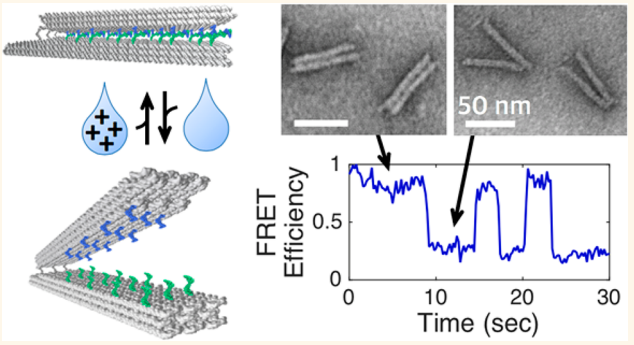

KEYWORDS: *DNA nanotechnology, DNA origami, statistical modeling, dynamic nanostructures, rapid actuation*

Controlling the motion of nanoscale structures is an essential step toward developing functional nanodevices and nanorobots that can have broad applications in fields ranging from nanomanufacturing to medicine. Recent advancements in DNA nanotechnology have led to complex nanoscale machinery and controllable dynamic devices including DNA walkers,[1−4] reconfigurable structures,[5−9] mechanical joints with well-defined rotational or translational degrees of freedom,[10−23] and multijoint mechanisms.[10,20,24,25] In some cases, these devices can be moved along a predefined motion path[2,3,13,18,20] or flipped between conformations,[13,16,17,20,24] showing promise for complex controllable DNA-based nanomachines.

While dynamic devices have rapidly evolved in structural and dynamic complexity over the past decade, methods for controlling such devices in a rapid and reproducible manner are lagging behind. The most commonly used method to control DNA devices, DNA strand displacement,[7] involves mixing devices with single-stranded DNA (ssDNA) that reconfigures a device by selectively displacing strands. This displacement releases double-stranded DNA (dsDNA) connections between components on a device (*e.g.*, a container and a lid). Often, the addition of another ssDNA strand that

Received: June 25, 2018
Accepted: August 31, 2018
Published: August 31, 2018

DOI: 10.1021/acsnano.8b04817
ACS Nano 2018, 12, 9484–9494

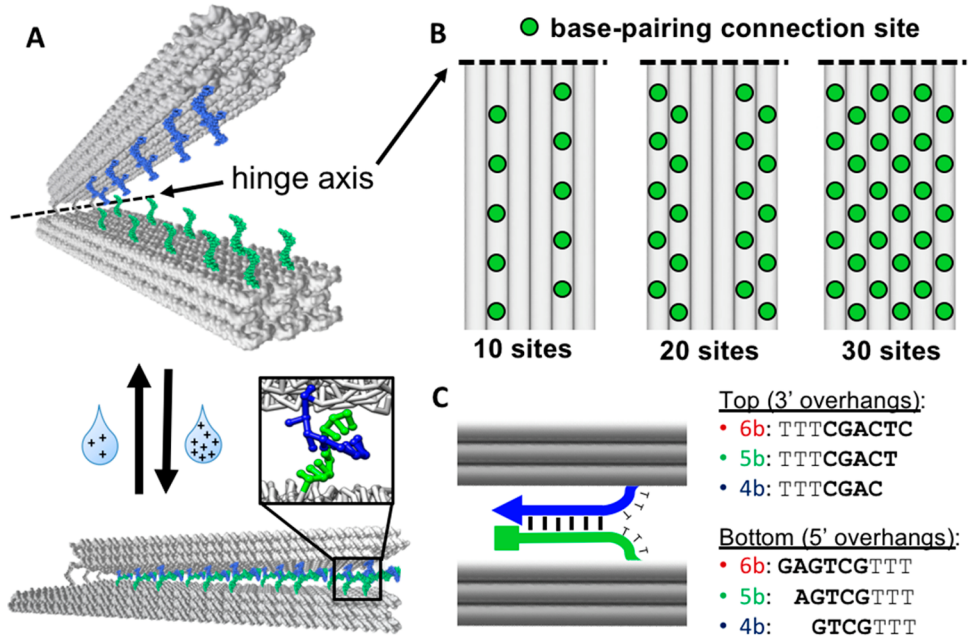

Figure 1. Ion-activated reconfigurable DNA nanostructures. (A) Short ssDNA overhangs (blue and green) protrude from the hinge arms. Overhang sequences are complementary to each other, but their free energy of hybridization is weak at low cation concentrations. Overhang hybridization is stabilized with increased cation concentration, and the overhangs collectively bind to close the hinge. (B) Overhang locations on the hinge arms for the three designs containing different numbers (10, 20, and 30 pairs) of connections. (C) All overhangs include a TTT linker for separation from the hinge. The square represents the 5′ end of the overhang, while the triangle represents the 3′ end. A total of three different overhang lengths (four, five, and six bases) were explored in this study.

hybridizes to the displacement site can re-establish the dsDNA connection enabling reversible and repeatable actuation.[7,26] The main advantages of strand displacement include sequence specificity, the relative ease of integrating DNA sites for actuation on a wide range of devices, and the potential to interface with molecular computation that relies on similar displacement reactions.[10,21,26,27] However, this approach is limited by the relatively slow time scales of actuation, typically minutes or longer. To address these challenges and to broaden the range of triggering mechanisms, recent efforts have demonstrated actuation using various biomolecules,[16,27−32] often using DNA aptamers for target specificity.[16,27,30,32] Applying forces through optical traps, atomic force microscopy, and centrifuge force microscopy have also been explored as possible mechanisms for manipulating DNA structures.[33−38] In addition, electrical[39] and magnetic[40] actuation methods have been implemented to enable control at sub-second time scales and in the case of the electrical actuation control at speeds up to tens of Hz. These approaches require external inputs and some advanced system or assay fabrication.

Many applications (for instance, in biomedicine) may require less-invasive approaches for actuation or devices that can respond to a variety of cues in the local environment. Indeed, emerging studies have begun to actuate DNA nanostructures using light and environmental changes such as temperature, pH, and ion concentrations through the incorporation of azobenzene moieties,[41,42] DNA base-stacking interactions,[13] G quadruplexes,[16] and DNA triplex-forming motifs[43] into the DNA nanostructures. In particular, Kuzyk *et al.*[43] developed a pH-triggered mechanism demonstrating the ability to engineer range of sensitivity, and Gerling *et al.*[13] developed ion-based actuation of dynamic devices that mediated base-stacking interactions within the devices. Both studies used bulk fluorescence methods to demonstrate response on ∼10 s time scales.

Here, we introduce a simple and tunable strategy for rapid actuation of DNA nanostructures featuring sub-second transitions and second-scale temporal resolution of repeated actuation, as revealed by single-molecule measurements of triggered conformational changes. Our method combines an engineered response to environmental changes with sequence-specificity of DNA hybridization for reconfiguring structures. We achieve this by modifying DNA structures with short ssDNA sticky ends that rapidly hybridize or dehybridize in response to changes in concentration of specific cations, enabling the large-scale reconfiguration of structures within short time scales. We demonstrate the utility of this approach by actuating DNA hinge nanodevices using several different cations, achieving reversible and repeatable opening and closing of hinge arms within sub-second time scales. We further show the ability to tune the actuation response and to quantitatively model its behavior as a function of cation concentration and a number of design parameters, thereby providing a rational means to engineer the sensitivity and range of the actuation response. Given the straightforward and inexpensive incorporation of ssDNA overhangs, this approach is readily extendable to a variety of devices. In addition to actively actuating nanodevices, this approach may also be used in a passive form, for instance, as calibrated sensors to measure ion concentrations. The method presented here should therefore provide a valuable tool for researchers aiming to introduce dynamical mechanisms into otherwise static DNA nanostructures.

The over-arching principle of our actuation method, similar to that of many existing approaches, is a switchable affinity between structural components that can be turned on or off *via* addition or removal of an external trigger, enabling structures

DOI: 10.1021/acsnano.8b04817
ACS Nano 2018, 12, 9484−9494

to be actuated between conformations with well-separated ("open" state) and latched together components ("closed" states). In our approach, the affinity is generated by introducing a number of short, mutually complementary ssDNA strands (overhangs) across the surfaces of the components to be actuated. The overhang sequence can be added to the end of an existing staple at the appropriate spatial position and helical twist orientation to ensure that the overhangs protrude from the surface in an appropriate location and direction to bind to its complementary strand on the opposing surface. In contrast to prior approaches that leverage base-pairing interactions, we use short overhang sequences that individually are too weak to stably hybridize at room temperature. However, the collective binding energy of many distributed overhang binding sites (*i.e.*, avidity) allows these short sequences to form connections between components that become thermodynamically stable at cation concentrations that are high enough to sufficiently screen electrostatic repulsions between the phosphate backbones of the interacting overhangs.[44] Thus, by raising or lowering the cation concentration, the structure can be actuated to close or open, respectively.

There are two key aspects of this approach that enable rapid actuation response. First, the actuating strands remain localized on the device, so they effectively remain at very high local concentrations. Second, the low affinity of individual strands means that they should quickly dissociate upon lowering cation concentrations without any need for strand displacement, which is a relatively slow process. This enables significantly faster actuation rates compared with methods in which actuating strands are introduced into the solution, typically at submicromolar concentrations, and have to undergo a diffusive search process before hybridizing with their target. The only diffusive mechanism at play in our approach is that of the cations, which occurs at a faster time scale than strand diffusion due to their small size and much higher concentrations (millimolar instead of nanomolar). Furthermore, the overhangs are likely to exhibit collective hybridization because they are aligned across the actuated components.

To demonstrate and characterize our ion-based actuation method, we applied it to a set of previously reported DNA origami hinges.[20] The hinges are composed of two stiff arms, each a rectangular bundle of 18 dsDNA helices organized in a 3 × 6 square lattice cross-section.[45] The arms are connected by several flexible ssDNA scaffold connections arranged in a line to form the hinge rotation axis. We previously showed[20] that the hinge arms rotate flexibly over a range of angles, exhibiting largely open conformations. To enable ion-triggered actuation between such open conformations and a closed conformation, we modified these hinges to include short ssDNA staple overhangs distributed along the inner face of each arm at complementary locations (Figures 1A and S1). In this study, we used a range of cationic triggers, and explored the use of 10 to 30 overhangs on each arm with sequence lengths ranging from 4 to 6 bases for both hinge designs (Figure 1B,C). We also explored two versions of the hinges termed "Hinge1" and "Hinge2" that we previously showed[20] to differ in torsional stiffness of the hinge joint, with Hinge1 exhibiting a higher resistance to closing than Hinge2.

RESULTS AND DISCUSSION

Cation-Activated Actuation of DNA Origami Hinges.

Before studying cation-mediated actuation of the overhang-modified DNA hinges, we first examined the effects of cation concentration on the original hinges (without overhangs). The reason is that in addition to altering the affinity of the overhangs for hybridization, changing ion concentrations could also influence the internal structure and conformational dynamics of the hinge itself. To rule out such possible direct effects of ion concentrations on hinge mechanics, we measured the angular distributions from transmission electron microscopy (TEM) images of the original hinges for a range of ion concentrations. Free-energy landscapes were obtained from the measured distributions assuming a Boltzmann factor weighting as we have previously done.[19,20,22] For the span of $MgCl_2$ concentrations (5−40 mM) in which we examined the actuation response, we observe almost no effect on the inferred free energy profiles (Figures 2 and S2). This

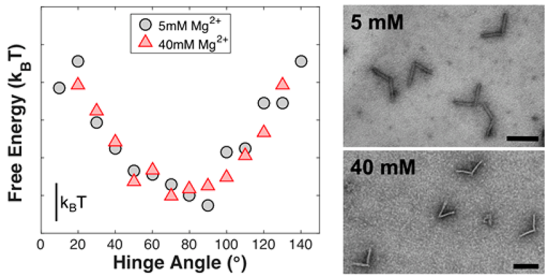

Figure 2. Conformational dynamics of freely fluctuating hinges without overhangs are not directly affected by changes in Mg^{2+} conditions. Scale bar: 100 nm.

concentration range was selected to ensure stability of DNA origami and avoid excessive aggregation of the structures. In contrast, we observe a slight effect on the free energy landscape while varying NaCl concentrations in the range of 0.2−1.4 M (Figure S3). Spd (50−120 μM) also shows little effect on energy landscape (Figure S4). Our results illustrate that changes in ion concentrations minimally influence the energy landscape of the hinges; hence, any actuation of the hinge angle should be a result of the influence of ions on the interactions between the overhangs.

Next, we studied the actuation behavior of the overhang-modified hinges as a function of varying ion concentrations. We focused on four design variables that modulate the actuation response of our devices: the number of overhang connections, the strength of these connections (number of complementary base pairs across overhangs), the torsional stiffness of the hinge (Hinge1 versus Hinge2), and the cation used. Magnesium was chosen to demonstrate the effects of the first three parameters because it is the most commonly used ion for stabilizing DNA origami[46,47] and because it does not influence the energy landscape of the hinges as shown by our analysis above. Importantly, when constructing hinges with varying numbers and lengths of overhangs, we used the same base hinge design with the only changes being the selection of staple strands with and without overhang extensions at appropriate locations. We quantified the equilibrium actuation response of each of these hinges through TEM analysis by measuring the fraction of hinges that close as a function of varying ion concentrations in solution. Because completely closed hinges are rarely achieved without overhangs (Figures

DOI: 10.1021/acsnano.8b04817
ACS Nano 2018, 12, 9484−9494

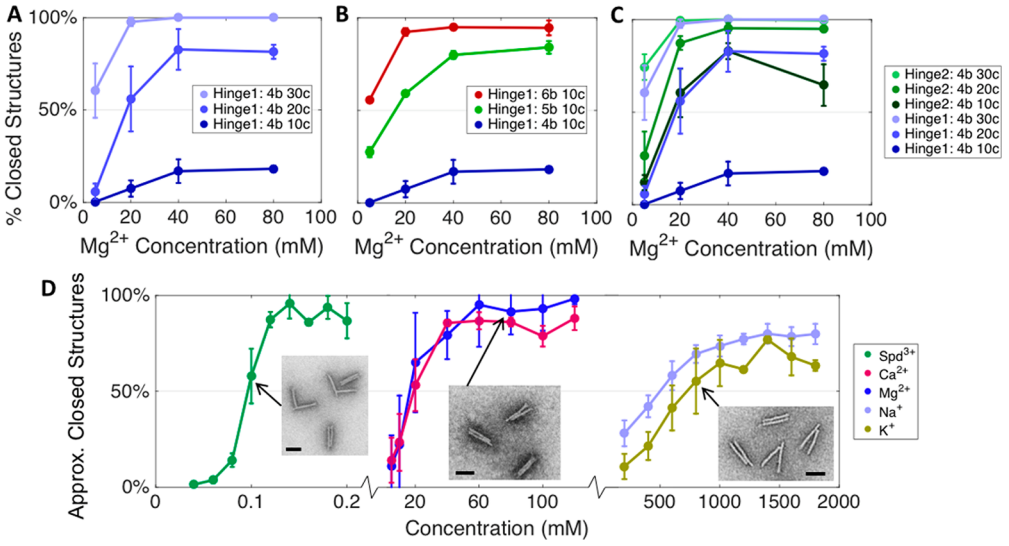

Figure 3. Experimental actuation responses measured as percentage of closed hinges vs ion concentration for a range of hinge designs and ions. The actuation responses are sensitive to (A) the number of overhang connections, (B) the length of overhangs, (C) the hinge stiffness, and (D) the valence charge of the cation. The first number in the data legends corresponds to the hinge design number, with Hinge1 being rotationally stiffer than Hinge2, the second number corresponds to the length of the overhangs (*e.g.*, 4b ≡ 4 bases), and the last number denotes the number of connections (*e.g.*, 10c implies 10 overhangs on the top arm and 10 complementary overhangs on the bottom arm). All hinges in panel D are Hinge2 with a total of 10 4-base connections. Data in panels A–C was measured *via* TEM. Data in panel D were obtained *via* ensemble FRET, while select samples were also counted from TEM. The TEM data were used to calculate a linear relationship between FRET efficiency and closed hinge fraction. Details of the transformation are shown in Figure S6. Scale bars: 50 nm.

S2–S5), hinges that were actuated into a completely closed conformation were easy to distinguish from un-actuated hinges in TEM images.

Figure 3A shows the impact of changing the number of connections distributed across the hinge arms. These hinges all have 4-base overhangs and explore the full spectrum of conformational compositions ranging from 0% to 100% closed structures with 10 to 30 connections and 5 to 80 mM $MgCl_2$ concentrations. For each hinge, the fraction of closed structures rises sharply with increasing ion concentration at low concentrations before slowing down and saturating at higher concentrations to a plateau value indicative of the maximum yield of closed hinges attainable with that particular number and arrangement of weak connections. The actuation responses become sharper (*i.e.*, more sensitive to ion concentration) and yield higher fractions of closed structures (at all ion concentrations including saturation values) with increasing number of connections. Another design parameter that alters the sensitivity to ion concentrations is the length of the overhangs. Figure 3B shows this effect for various 10-connection hinges, where adjusting the overhang length from 4 to 6 bases leads to a sharper actuation response and higher yield of closed structures, effects similar to those obtained with increasing number of connections. Interestingly, the hinge with 10 5-base connections yields a similar saturation yield of closed hinges as the hinge with 20 4-base connections, but the 20 4-base connections exhibit a different sensitivity to ion concentration at low salt conditions. These results reveal an ability to engineer both the sensitivity and range of the actuation response.

Changing the number or length of connections are simple design parameters that are easily adjusted by substituting several staples in the hinge design during the self-assembly reaction. We also studied the effect of the torsional stiffness of the hinge, which determines its resistance to closing. Torsional stiffness was varied by altering the ssDNA joint connections using a different hinge design.[20] Figure 3C illustrates the effect of hinge stiffness on actuation using structures having four-base overhangs on each arm. Our results show that Hinge2, which has a lower stiffness than Hinge1, yields a steeper actuation response that is also shifted to lower ion concentrations, suggesting that hinge stiffness is an additional design parameter that controls the range and sensitivity of the actuation response. In addition, these results illustrate that mechanical properties are a key consideration in determining device functional response.

We further characterized the ability to actuate the hinges using a variety of other mono-, di-, and trivalent cations including K^+, Na^+, Ca^{2+}, and Spd^{3+}. To enable rapid measurement over a broad range of ion concentrations, we folded one version of Hinge2 (10 connections, each 4 bases long) with a donor and acceptor fluorophore on opposite arms to enable a Förster resonance energy transfer (FRET) readout of the closed hinges. We analyzed multiple samples by both ensemble FRET and by TEM imaging to calibrate the FRET efficiency in terms of fraction of closed hinges. Our analysis revealed a linear relationship between the two quantities for each cation, which was then used to transform FRET efficiency to closed fraction of hinges for all samples (Figure S6). Our results shown in Figure 3D indicate that the sensitivity of the hinges to actuation rises drastically with the valence charge on the ions, consistent with their increasing electrostatic screening effect (*i.e.*, decreasing Debye lengths). In other words, rapidly diminishing concentrations of mono-, di-, and trivalent ions (~200–1000 mM, ~5–40 mM, and ~0.06–0.14 mM, respectively) are required to achieve similar levels of actuation (~20 to 80% of closed hinges). That different cations of the same charge (*e.g.*, Mg^{2+}/Ca^{2+} and Na^+/K^+) produce similar actuation responses confirms an electrostatics-based effect of

DOI: 10.1021/acsnano.8b04817
ACS Nano 2018, 12, 9484–9494

ions on DNA hybridization. Additional TEM images of these hinges are available in Figure S7.

Theoretical Model of Actuation Response. To explain the observed actuation behavior and its dependence on the hinge design parameters studied above, we developed a quantitative model that relates the probability P_{closed} of observing a closed hinge to the ionic concentration c. The model classifies the ensemble of hinge conformations in terms of two states: a "closed" state describing conformations with sufficiently small hinge angles that permit overhang hybridization and an "open" state describing all remaining conformations. According to equilibrium statistical mechanics, $P_{closed} = Z_{closed}/(Z_{open} + Z_{closed})$, where Z_{closed} and Z_{open} are the partition functions associated with the two states. Assuming that the n overhangs on each hinge arm are indistinguishable and that each overhang interacts only with its complementary counterpart on the opposite arm, Z_{closed} and Z_{open} can each be partitioned into two terms. The first is a bare-hinge partition function related to conformations of the hinge without overhangs in the two respective states. The second is a product of n identical overhang partition functions related to conformations of each pair of overhangs, *i.e.*, partly to fully hybridized conformations in the closed state and unassociated conformations in the open state. Relating the bare-hinge and overhang partition functions to free-energy changes associated with bare-hinge rotation and strand hybridization then yields the following relationship:

$$P_{closed}(c) = \frac{\left[1 + \exp\left(-\frac{\Delta G_{hyb}(c) + \Delta G_{fix}}{RT}\right)\right]^n}{\left[1 + \exp\left(-\frac{\Delta G_{hyb}(c) + \Delta G_{fix}}{RT}\right)\right]^n + \exp\left(\frac{\Delta G_{bh}}{RT}\right)}$$

where $\Delta G_{hyb}(c)$ is the free energy of hybridization of each overhang pair in solution, ΔG_{fix} is a correction to this free energy that accounts for entropy loss due to the confinement from the hinge arms, ΔG_{bh} is the free energy change of a bare hinge undergoing transition from an open to a closed state, R is the universal gas constant, and T is the temperature. A detailed derivation of this relationship is provided in the Supporting Information.

Based on known logarithmic dependence of ΔG_{hyb} on ion concentration,[48,49] the above model predicts that the fraction of closed hinges rises from a value of $P_{closed} = [1 + \exp(\Delta G_{bh}/RT)]^{-1}$ at $c = 0$ to the asymptotic value of 1 at $c \to \infty$. This prediction agrees well with the shape of the experimentally observed actuation responses. The functional form of the model further predicts that strongly negative $\Delta G_{hyb}+\Delta G_{fix}$ (long overhangs), large n (many overhangs), and small ΔG_{bh} (small energy barrier for bare hinge closing) all contribute to increasing ion sensitivity of the hinges, also consistent with the experimentally observed trends. Finally, the model suggests that to shift the range of the actuation response to higher ion concentrations, the energy barrier between the closed and open state of the bare hinge should be sufficiently large. The functional form of our model is thus already capable of qualitatively explaining the observed actuation behavior and demonstrating the crucial roles of both the hinge joint and the overhangs in sharpness and range of the actuation responses.

We next investigated the ability of this model to quantitatively fit the experimental actuation responses shown in Figure 3A–C for the eight distinct hinge designs differing in terms of the number of overhangs, overhang lengths, and hinge stiffness. This data obtained using $MgCl_2$ represents our broadest data set and also shows minimal changes to the intrinsic free energy landscape across a wide range of concentrations (Figure S2). Furthermore, the solution-state free energies of hybridization ΔG_{hyb} are readily available for Mg^{2+} as a function of its concentration. In this study, we obtained these free energies from the DINAMelt server, part of the DNA/RNA secondary structure prediction software UNAFold.[48,49] We then minimized the weighted sum of squared errors between the model and experimental data, varying the two remaining unknown parameters ΔG_{bh} and ΔG_{fix}. ΔG_{bh} was kept unchanged across hinges with the same joint stiffness, and ΔG_{fix} was kept unchanged across hinges carrying the same number and length of overhangs. Figure 4 presents our results from simultaneous fitting of all actuation profiles. A coefficient of determination (R^2) value of 0.96 and a p value of 0.993 for the chi-square test indicates excellent agreement between model and experiment, especially considering that the two fit parameters were fixed across groups of hinges with similar stiffness or overhang lengths. The model also accurately predicts the NaCl actuation response (Figure S8).

The fitted values of ΔG_{bh} and ΔG_{fix} obtained for the different hinge designs make physical sense. We obtained ΔG_{bh} = 2.80 and 1.39 kcal/mol for Hinge1 and Hinge2, respectively. The positive values of ΔG_{bh} are consistent with the open state being more prevalent than the closed state in bare hinges (see Figures S2 and S3), and the larger value for Hinge1 is consistent with stiffer hinges displaying a larger energetic penalty for closing. Furthermore, the free energy difference obtained for Hinge1 is close to the value of 3.59 kcal/mol estimated from our experimental angular distributions using the ratio between numbers of bare hinge configurations presenting open and closed states with a threshold of 10°, *i.e.*, $\Delta G_{bh} \approx -RT \ln(N_{open}/N_{closed})$ (see Figure S9). We obtained ΔG_{fix} = 6.07, 6.12, and 5.99 kcal/mol for hinges with 10, 20, and 30 overhang pairs with 4 complementary bases, respectively, and 7.35 and 8.24 kcal/mol for hinges with 10 overhang pairs with 5 and 6 complementary bases, respectively. The positive values of ΔG_{fix} are reasonable considering that the hybridization of overhangs is impaired due to confinement effects; that is, the steric constraints imposed by the hinge arms significantly reduce the configurational and rotational entropy of the overhangs in the hinge closed state. We also note that ΔG_{fix} is largely independent of the number of overhangs on each hinge arm, suggesting that the overhang length and surface density are sufficiently small that they do not interact with each other, consistent with one of the assumptions of our model. That ΔG_{fix} increases in magnitude with the degree of complementarity (length of overhangs) suggests that the entropic penalty imposed by the arms on the overhangs is stronger for longer strands.

Characterization of Actuation Dynamics. A key advantage of actuating DNA devices using ion-mediated control of localized overhangs is the potential for fast response. To investigate the opening and closing kinetics of our ion-activated hinges, we used a single-molecule FRET (smFRET) assay on a total internal reflection fluorescence (TIRF) microscope (Figure 5A). In this approach, the hinges were folded with a pair of donor and acceptor fluorophores attached to the inner surfaces of the hinge arms, so the FRET signal is an indication of hinge configuration. In addition, hinges incorporated biotinylated overhangs extending from the outer

DOI: 10.1021/acsnano.8b04817
ACS Nano 2018, 12, 9484–9494

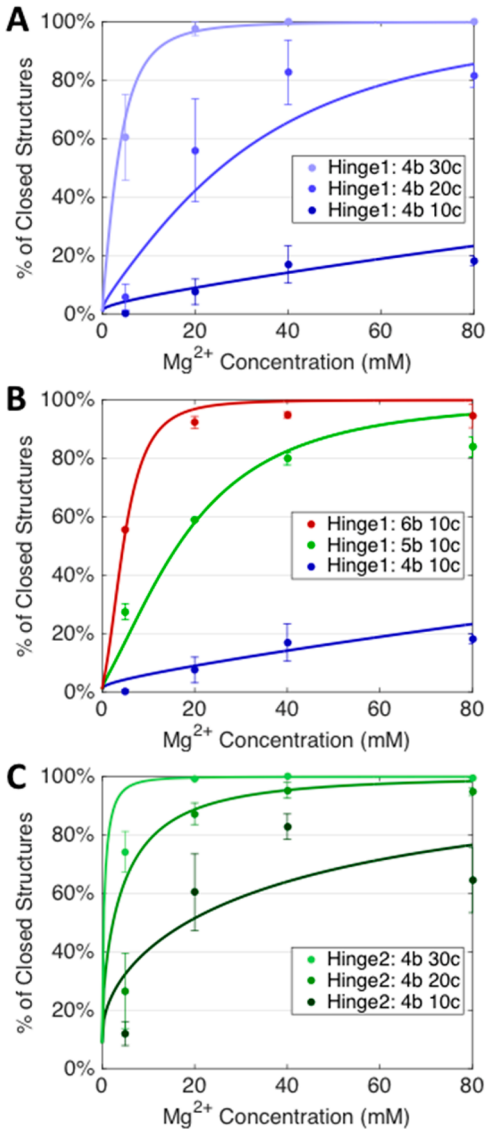

Figure 4. Model fits to experimental actuation response curves. Experimental data for different hinge designs are shown in symbols, and the model fits are shown as solid lines of same color as the fitted data. The data legends format is identical to that in Figure 2, where the three numbers correspond to the hinge design, the length of the overhangs, and the number of connections. The fitting procedure yielded ΔG_{bh} = 2.80 and 1.39 kcal/mol for hinges with joint designs 1 and 2 and ΔG_{fix} = 6.07, 6.12, and 5.99 kcal/mol for hinges with 10, 20, and 30 overhang pairs, each with 4 complementary bases, and ΔG_{fix} = 7.35 and 8.24 kcal/mol for hinges with 10 overhang pairs with 5 and 6 complementary bases, respectively.

surface of one of the arms to provide a way to immobilize the DNA hinges onto a glass coverslip while allowing them to open and close freely based on solution conditions. A flow channel system was used to change solutions in real time while monitoring the opening and closing of the hinges based on the FRET efficiency readouts. In short, two syringe pumps connected to the channel inlet were used to change solutions in the flow channel. The pumps were controlled manually. Extended details of this assay are explained in the Materials and Methods section. Using this approach, we examined the opening-closing dynamics of Hinge2 with 20 4-base overhang connections. Hinges were initially observed at low $MgCl_2$ concentrations of 5 mM, in which they were expected to be largely open. At these concentrations, the smFRET signals were observed to be consistently low. To test the actuation, we observed the hinges in the open state for ∼5−10 s and then manually triggered the syringe pump to flow in high $MgCl_2$ concentration buffer (40 mM). We observed abrupt increases in the FRET efficiency a few seconds after triggering the syringe pump, signifying the closed transition (Figure 5B). The few seconds delay (∼1−3 s) reflected the time required for the buffer exchange and varied slightly depending on the position in the flow channel. Similarly, Figure 5C shows a closed hinge in a high $MgCl_2$ solution (high FRET efficiency) opening as a low $MgCl_2$ solution is flowed into the channel using a similar approach. Additional sample traces of closing and opening transitions are provided in Figure S10. As important controls, we verified that these transitions do not occur when buffer with the same ion concentration is flowed into the channel or when ion concentrations were changed, but hinges did not contain overhangs (Figure S11). These results demonstrate reversible actuation of hinges between open and closed states and also illustrate that actual structural transitions from open to closed or closed to open occur on millisecond time scales ($\lesssim$ 200 ms), and the control time is limited the time required for the initial buffer exchange.

To demonstrate the reversibility and repeatability of hinge actuation, we implemented alternating low and high $MgCl_2$ solutions in the channel. Hinges were again observed in the open state followed by manually activating the syringe pumps to change the buffer conditions between 5 mM and 40 mM $MgCl_2$ every few seconds. As demonstrated in the traces presented in Figure 5D,E (and in the additional traces at different frequencies provided in Figure S10), we obtained repeatable opening and closing of the hinges prior to photobleaching. Note that in these experiments, the cycle time is again limited to seconds due to the time required to exchange buffers with different ion concentrations and not by the actuation response time of the hinges. While manually alternating between high and low $MgCl_2$ solutions every few seconds, we see smFRET transitions at the same time scale, while the actual transitions themselves occur faster than our time resolution (200 ms). Overall, these results demonstrate direct visualization of reversible and repeatable millisecond time scale changes in the conformation of DNA devices in response to local changes in ion concentrations.

CONCLUSIONS

The work presented here demonstrates a simple and robust method for rapid actuation of DNA-origami devices based on ion-mediated hybridization of multiple short ssDNA strands introduced into the device. This method leverages multivalent interactions between components wherein the individual interactions are driven by weak DNA base pairing that is sensitive to local ion concentrations. In this manner, devices can be reconfigured based on changes in ion concentration without the need for binding DNA components from solution or displacing DNA strands from the structure. These features enable the rapid, triggerable reconfiguration of structures on millisecond time scales, as revealed by monitoring the actuation of individual devices in real-time using smFRET assays. The response time is faster than those achieved by the most commonly used approach for actuation, DNA strand displacement, which is typically on the time scale of minutes or greater.[13,20] We further demonstrated the ability to trigger

DOI: 10.1021/acsnano.8b04817
ACS Nano 2018, 12, 9484−9494

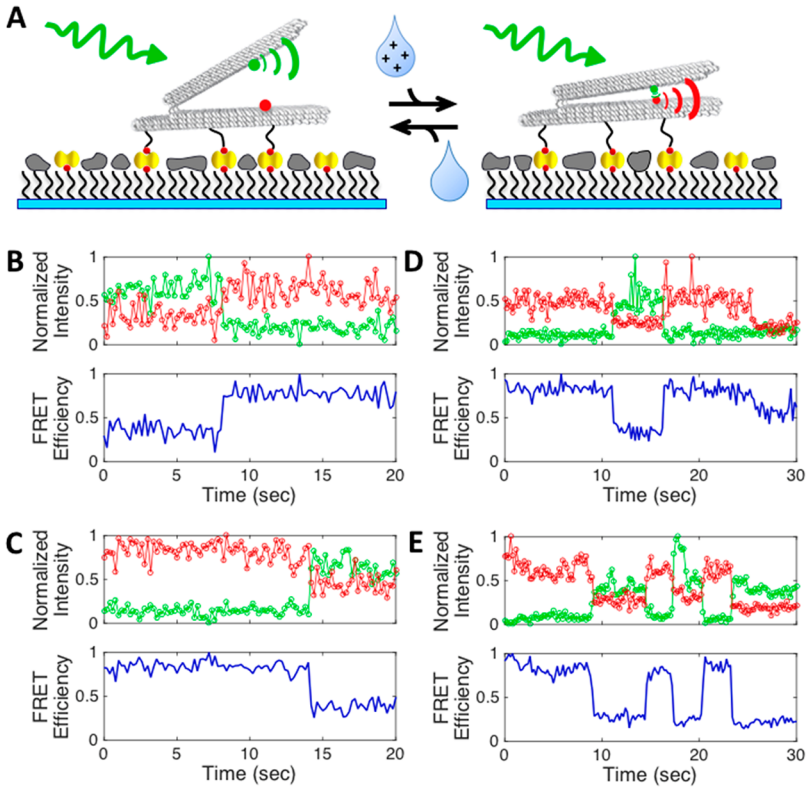

Figure 5. Dynamics of hinge actuation captured *via* smFRET. The schematic in panel A shows hinge attachment to a biotin−PEG functionalized coverslip through biotin−streptavidin binding. Representative traces are shown for hinge (B) closing, (C) opening, and (D, E) alternate opening-closing at different speeds. Green data correspond to the donor signal, red data correspond to the acceptor signal, and blue lines show the calculated relative FRET efficiency.

successive reconfigurations with temporal resolution on the second-scale. However, because the transitions are relatively fast, the time resolution for actuation could likely be further shortened to at least the ∼100 ms time scale with more advanced microfluidics[50] or ionically active materials[51] for modulating local ion conditions.

The actuation method is highly tunable, and we demonstrated that the number and strength of connections along with the torsional stiffness of the hinges could be used to tune the response to desired ion concentrations. Importantly, engineering the actuation response only requires minor design modifications that are easily implemented on a baseline design by substituting a few staple strands. The actuation response and its dependence on the strength of overhangs connections and hinge stiffness can be well-described by a simple statistical-mechanical model based on the interplay between the free energies associated with overhang hybridization and hinge rotation. This ability to model and predict actuation responses based on design parameters should enable a rational design approach to tuning and optimizing the actuation method. In addition, the model explains how mechanical properties of the structures can be used to engineer the actuation response. While we demonstrated this actuation method by opening and closing hinges, the approach is readily extendible to other kinds of devices or structural transitions, provided there are components that can be reconfigured through the hybridization/dissociation of overhangs. The method is straightforward to implement thereafter as the overhang placement can be accomplished without major modifications to the original DNA origami design.

This work joins a series of recent advances using dynamic DNA devices to exhibit actuation triggered by a variety of inputs at time scales significantly faster than previous approaches. In particular, external electrical[39] and magnetic[40] fields enable precise control over rotational devices on subsecond time scales, but these approaches require external components for control. Solution-based triggers utilizing pH-responsive DNA complexes[43] and base stacking interactions sensitive to cation concentration[13] have been demonstrated as approaches to allow actuation in response to environmental changes at the time scale of ten seconds. The ion-actuation method we have presented here enables rapid transitions at sub-second time scales, as directly revealed by single-molecule methods, with a tunable ion-based actuation response. Because our approach requires minimal modifications to DNA origami devices, it can be easily adopted to a range of devices with our theoretical model as a guide. Moving forward, it is likely that future generations of complex DNA nanorobots and systems will require integration of multiple actuation methods encompassing reconfiguration of structures that are externally driven and responsive to environmental conditions with a variety of triggering mechanisms.

MATERIALS AND METHODS

Design, Fabrication, and Basic Characterization. DNA-origami structures were designed using cadnano,[52] and unique overhang sequences were designed using MATLAB. Potential hairpins, homodimers, and complementarity to other single-stranded DNA exposed on the structures were avoided when designing overhang sequences. Structures were formed following procedures from Castro *et al.*[53] Briefly, 7560-nt (Hinge1) or 8064-nt (Hinge2)

DOI: 10.1021/acsnano.8b04817
ACS Nano 2018, 12, 9484−9494

scaffolds were produced in lab and mixed at 20 nM with staple oligos (Eurofins MWG Operon USA and Integrated DNA Technologies, Inc.) at 200 nM in a 1 mM EDTA, 5 mM Tris, 5 mM NaCl, and 18 mM $MgCl_2$ solution. The solution was subjected to rapid heating to 65 °C then slowly cooled in a thermal annealing ramp over ∼2 days to 25 °C.

Actuation Response. Structures were purified using polyethylene glycol (PEG) precipitation with buffer exchange[54] and then adjusted to the desired ion concentration plus a residual 1 mM $MgCl_2$. All experiments were performed at room temperature. Samples were prepared for TEM following protocols in Castro *et al.*[53] and imaged on a FEI Tecnai G2 Spirit TEM. Aggregation was seen in TEM for calcium samples and for other ions at high concentrations. Vortexing and repeated pipetting helped to break up aggregates for TEM sample preparation. TEM images were measured using ImageJ. Hinges deposited on their wide surface were not included in this analysis because their conformation is unattainable. Bulk fluorescence intensity was measured using a FluoroMax-4 spectrofluorometer (Horiba Scientific), and ensemble FRET efficiency was calculated using the following equation to account for direct acceptor excitation from the donor wavelength light: $E = (I_{AD}A_{AA} - I_{AA}A_{AD})/I_{AA}A_{DD}$, where I is the measured intensity, A is the measured absorbance, and the subscripts correspond to the recorded emission wavelength followed by wavelength of excitation [acceptor (A) or donor (D)].

Model Development. The probability P_{closed} of the hinge exhibiting a closed state may be obtained from the partition functions Z_{closed} and Z_{open} of the closed and open states:[55]

$$P_{closed} = \frac{Z_{closed}}{Z_{closed} + Z_{open}} \tag{1}$$

where the two partition functions, by definition, are given by:

$$Z_{closed} = \sum_{\mathbf{r}_h, \mathbf{r}_s \in closed} \exp[-E(\mathbf{r}_h, \mathbf{r}_s)/k_BT] \tag{2}$$

$$Z_{open} = \sum_{\mathbf{r}_h, \mathbf{r}_s \in open} \exp[-E(\mathbf{r}_h, \mathbf{r}_s)/k_BT] \tag{3}$$

Here, k_B is the Boltzmann constant, T is the temperature, and $E(\mathbf{r}_h, \mathbf{r}_s)$ is the total energy of the hinge, which is a function of the set of coordinates $\mathbf{r}_h$ describing the conformation of the bare hinge (without ssDNA overhangs) and the coordinates $\mathbf{r}_s$ describing the conformation of all ssDNA overhangs. The summations in eqs 2 and 3 are carried out over the ensemble of hinge conformations belonging to the closed and open states.

We next make the assumption that the total energy of the hinge can be effectively decoupled into an energy term, E_h, that is the function of the bare hinge conformation alone and another energy term, E_s, that is a function of the ssDNA overhang conformations only:

$$E(\mathbf{r}_h, \mathbf{r}_s) \approx E_h(\mathbf{r}_h) + E_s(\mathbf{r}_s) \tag{4}$$

This assumption, implemented in many statistical mechanical models, allows the overall partition functions in eqs 2 and 3 to be written as the product of the partition function of the two subsystems (the bare hinges and the overhangs):

$$Z_{closed} = Z_{h,closed} \times Z_{s,closed} \tag{5}$$

$$Z_{open} = Z_{h,open} \times Z_{s,open} \tag{6}$$

where $Z_{h,closed}$ and $Z_{s,closed}$ are the partition functions of the closed state of the bare hinge and the overhang strands, and $Z_{h,open}$ and $Z_{s,open}$ are the partition functions of the open state for the two subsystems:

$$Z_{h,closed} = \sum_{\mathbf{r}_h \in closed} \exp[-E(\mathbf{r}_h)/k_BT]$$

$$Z_{s,closed} = \sum_{\mathbf{r}_s \in closed} \exp[-E(\mathbf{r}_s)/k_BT] \tag{7}$$

$$Z_{h,open} = \sum_{\mathbf{r}_h \in open} \exp[-E(\mathbf{r}_h)/k_BT]$$

$$Z_{s,open} = \sum_{\mathbf{r}_s \in open} \exp[-E(\mathbf{r}_s)/k_BT] \tag{8}$$

By recognizing that the ratio $Z_{h,closed}/Z_{h,open}$ is intrinsically related to the free energy change of the bare hinge undergoing transition from the open to the closed state *via*

$$\Delta G_{bh} = -k_BT \ln(Z_{h,closed}/Z_{h,open}) \tag{9}$$

the expression for the closed-state probability in eq 1 can now be simplified based on eqs 5, 6, and 9 to:

$$P_{closed} = \frac{(Z_{s,closed}/Z_{s,open})}{(Z_{s,closed}/Z_{s,open}) + \exp(\Delta G_{bh}/k_BT)} \tag{10}$$

where the free-energy change ΔG_{bh} is assumed to be largely independent of Mg^{2+} concentration based on our experimental observations.

To estimate the ratio of the overhang partition functions in eq 10, we assume that each overhang, out of a total of n overhangs per hinge arm, can interact and hybridize only with its corresponding overhang on the other hinge arm and that the n pairs of overhangs are identical but distinguishable from each other. In this "ideal" scenario, the partition functions $Z_{s,\,closed}$ and $Z_{s,\,open}$ for a *system* of n pairs of overhangs can be written down in terms of the partition functions $Z^{(1)}_{s,\,closed}$ and $Z^{(1)}_{s,\,open}$ for a *single* pair of overhangs:

$$\frac{Z_{s,closed}}{Z_{s,open}} = \left(\frac{Z^{(1)}_{s,closed}}{Z^{(1)}_{s,open}}\right)^n \tag{11}$$

where $Z^{(1)}_{s,open}$ sums over all possible conformations of the two overhangs in the dissociated state, while $Z^{(1)}_{s,closed}$ sums over all possible conformations of the two overhangs in both hybridized and dissociated states. If one denotes the above sums over dissociated and hybridized states by Z_{dis} and Z_{hyb}, then:

$$\frac{Z_{s,closed}}{Z_{s,open}} = \left(\frac{Z_{hyb} + Z_{dis}}{Z_{dis}}\right)^n \tag{12}$$

where the ratio Z_{hyb}/Z_{dis} is related to the free energy of hybridization $\Delta G_{hyb,\,f}$ of a single pair of overhangs from the dissociated state while remaining fixed to the hinge arms:

$$\frac{Z_{hyb}}{Z_{dis}} = \exp\left(-\frac{\Delta G_{hyb,f}(c)}{k_BT}\right) \tag{13}$$

To obtain $\Delta G_{hyb,f}$, one can take advantage of available DNA/RNA secondary-structure prediction algorithms that provide the free energy of hybridization of the overhangs in solution as a function of Mg^{2+} concentration, which we denote by $\Delta G_{hyb}(c)$. To account for the entropy loss due to the confinement from the hinge arms, we add a concentration-independent correction term ΔG_{fix} to this free energy, whereby:

$$\Delta G_{hyb,f}(c) = \Delta G_{hyb}(c) + \Delta G_{fix} \tag{14}$$

Substituting eqs 12−14 into eq 10 then yields our final expression for the closed-state probability given by:

$$P_{closed} = \frac{\left[1 + \exp\left(-\frac{\Delta G_{hyb}(c) + \Delta G_{fix}}{RT}\right)\right]^n}{\left[1 + \exp\left(-\frac{\Delta G_{hyb}(c) + \Delta G_{fix}}{RT}\right)\right]^n + \exp\left(\frac{\Delta G_{bh}}{RT}\right)} \tag{15}$$

with two unknown parameters ΔG_{fix} and ΔG_{bh}. Note that we have replaced k_B with gas constant R so all free energies are in molar units.

Analysis of the Range and Sharpness of Actuation. We further analyzed the analytical expression for P_{closed} and its

DOI: 10.1021/acsnano.8b04817
ACS Nano 2018, 12, 9484−9494

dependence on the design parameters related to the ssDNA overhangs and bare hinges. For this purpose, we divided the solution-state hybridization free energy $\Delta G_{hyb}(c)$ into concentration-dependent and concentration-independent terms:

$$\Delta G_{hyb}(c) = -a_0 \ln c - b_0 \quad (16)$$

where a_0 and b_0 are positive parameters provided by the UNAFold package[48,49] related to the strength of hybridization between the two ssDNA overhangs. By defining $a \equiv -a_0/RT$, $b \equiv \exp[-(\Delta G_{fix} - b_0)/RT]$, and $g \equiv \exp(\Delta G_{bh}/RT)$, the expression for the closed-state probability in eq 15 reduces to:

$$P_{closed} = \frac{(1 + bc^a)^n}{(1 + bc^a)^n + g} \quad (17)$$

and its first derivative with respect to concentration is given by:

$$\frac{dP_{closed}}{dc} = \frac{P_{closed}(1 - P_{closed})nab}{c^{1-a} + bc} \quad (18)$$

To obtain sharp actuation of the hinges, *i.e.*, large change in P_{closed} over a small change in Mg^{2+} concentration, the derivative dP_{closed}/dc should be large. Based on the observed actuation behavior, it is reasonable to assume that the dP_{closed}/dc should be large at intermediate values of P_{closed} (*e.g.*, 0.5). The expression in eq 18 then suggests that the derivative dP_{closed}/dc is large when either n is large, *i.e.*, the hinge arms are attached with a large number of overhangs, or when a or b are large, *i.e.*, the hybridization between the overhangs is strong due to larger number of complementary bases on opposing strands. In addition, to obtain "late" actuation, *i.e.*, sharp change in P_{closed} at large Mg^{2+} concentrations, *e.g.*, at values higher than the 5 mM typically used for assembling the DNA origami hinges. The expression in eq 17 indicates that the critical Mg^{2+} concentration associated with this sharp increase in P_{closed} is controlled by the parameter g. Specifically, to achieve actuation at high Mg^{2+} concentrations, a large value of g is required, *i.e.*, hinges with stiff joints exhibiting a large free energy difference (energy barrier) ΔG_{bh} between the open and closed state of their bare counterparts is required. Thus, the designs of both the hinge joint and the overhangs are critical to achieving sharp and late actuation.

Single-Molecule Characterization. Fluorescent imaging was performed on a Nikon TiE inverted TIRF microscope with a Dual-View (Optical Insights) light-splitting cube. Kinetics experiments used two syringe pumps to control flow of 5 and 40 mM $MgCl_2$ solutions. The syringe outputs were connected with a T-joint as so ensure rapid solution changes in the flow cell when the pumps were turned on and off simultaneously. The channel was made from machined acrylic, cut double-sided tape, and a coverslip. A glass coverslip was functionalized with polyethylene glycol and biotin, streptavidin was then added to bind to the biotin, and, finally, casein was added to block nonspecific binding. Hinges folded with FRET pairs and biotinylated overhangs on the bottom were added to bind to the streptavidin. Once the bottom hinge arm is attached, the top arm should be able to open and close freely based on the solution in the channel. The sample was illuminated with a 561 nm laser to excite the Cy3 donor fluorophore. If the hinge is open, this fluorophore fluoresces light in the green−yellow spectrum. If the hinge is closed, the close proximity of the donor and acceptor fluorophores allows for a transfer of energy to the Cy5 acceptor fluorophore, which then emits red light. Splitting and filtering the light allowed for detection of both the donor and the acceptor fluorescence intensity simultaneously. Anti-correlated changes in intensity, corresponding to changes in relative FRET efficiency, are indicative of structure conformational changes. The acceptor was also directly excited with a 640 nm laser in alternating frames to verify its presence. Alternating laser excitation (ALEX) was used at 100 ms per laser illumination (200 ms frame rate) to capture near real-time hinge dynamics. Direct donor emission, direct acceptor emission, and FRET (donor excitation − acceptor emission) were recorded. Photobleaching occurred after extended exposure to the lasers and also helped verify the presence of single hinge devices. Fluorescence data from each channel was recorded and analyzed using Nikon Elements and MATLAB. Image analysis included drift correction, background subtraction, and colocalized fluorophore detection. Relative FRET efficiency was calculated using normalized intensities of the donor and FRET signal: $E_{rel} = I_{FRET}/(I_D + I_{FRET})$. Direct acceptor intensity was also recorded to realize acceptor photobleaching. All figures were made using MATLAB, Matplotlib, Autodesk Molecule Viewer, Chimera, and SolidWorks.

ASSOCIATED CONTENT

Supporting Information

The Supporting Information is available free of charge on the ACS Publications website at DOI: 10.1021/acsnano.8b04817.

Figures showing a modified hinge design, angular distributions and inferred free-energy landscapes of bare hinges, sample TEM images, linear transformations of FRET efficiency, model fits, cumulative angular distribution, and FRET traces (PDF)

AUTHOR INFORMATION

Corresponding Authors

*E-mail: castro.39@osu.edu.

*E-mail: gaurav.arya@duke.edu.

ORCID

Alexander E. Marras: 0000-0001-8972-9532

Hai-Jun Su: 0000-0002-3132-0213

Gaurav Arya: 0000-0002-5615-0521

Carlos E. Castro: 0000-0001-7023-6105

Notes

The authors declare no competing financial interest.

ACKNOWLEDGMENTS

We thank the Campus Microscopy and Imaging Facility (CMIF) at The Ohio State University as well as B. Walter and members of the Castro and Arya laboratories. This work was supported by NSF award no. 1536862. M.L. III was partially supported by the William G. Lowrie Department of Chemical and Biomolecular Engineering at The Ohio State University. A.E.M. was partially supported through a Presidential Fellowship from The Ohio State University.

REFERENCES

(1) Bath, J.; Turberfield, A. J. DNA Nanomachines. *Nat. Nanotechnol.* **2007**, *2*, 275−284.

(2) Gu, H.; Chao, J.; Xiao, S. J.; Seeman, N. C. A Proximity-Based Programmable DNA Nanoscale Assembly Line. *Nature* **2010**, *465*, 202−205.

(3) Omabegho, T.; Sha, R.; Seeman, N. C. A Bipedal DNA Brownian Motor with Coordinated Legs. *Science* **2009**, *324*, 67−71.

(4) Pan, J.; Li, F.; Cha, T. G.; Chen, H.; Choi, J. H. Recent Progress on DNA Based Walkers. *Curr. Opin. Biotechnol.* **2015**, *34*, 56−64.

(5) Krishnan, Y.; Simmel, F. C. Nucleic Acid Based Molecular Devices. *Angew. Chem., Int. Ed.* **2011**, *50*, 3124−3156.

(6) Modi, S.; MG, S.; Goswami, D.; Gupta, G. D.; Mayor, S.; Krishnan, Y. A DNA Nanomachine That Maps Spatial and Temporal Ph Changes inside Living Cells. *Nat. Nanotechnol.* **2009**, *4*, 325−330.

(7) Yurke, B.; Turberfield, A. J.; Mills, A. P., Jr.; Simmel, F. C.; Neumann, J. L. A DNA-Fuelled Molecular Machine Made of DNA. *Nature* **2000**, *406*, 605−608.

(8) Yan, H.; Zhang, X.; Shen, Z.; Seeman, N. C. A Robust DNA Mechanical Device Controlled by Hybridization Topology. *Nature* **2002**, *415*, 62−65.

(9) Aldaye, F. A.; Sleiman, H. F. Modular Access to Structurally Switchable 3D Discrete DNA Assemblies. *J. Am. Chem. Soc.* **2007**, *129*, 13376−13377.

DOI: 10.1021/acsnano.8b04817
ACS Nano 2018, 12, 9484−9494

(10) Castro, C. E.; Su, H. J.; Marras, A. E.; Zhou, L.; Johnson, J. Mechanical Design of DNA Nanostructures. *Nanoscale* **2015**, *7*, 5913−5921.
(11) Dhakal, S.; Adendorff, M. R.; Liu, M.; Yan, H.; Bathe, M.; Walter, N. G. Rational Design of DNA-Actuated Enzyme Nanoreactors Guided by Single Molecule Analysis. *Nanoscale* **2016**, *8*, 3125−3137.
(12) Funke, J. J.; Dietz, H. Placing Molecules with Bohr Radius Resolution Using DNA Origami. *Nat. Nanotechnol.* **2016**, *11*, 47−52.
(13) Gerling, T.; Wagenbauer, K. F.; Neuner, A. M.; Dietz, H. Dynamic DNA Devices and Assemblies Formed by Shape-Complementary, Non-Base Pairing 3D Components. *Science* **2015**, *347*, 1446−1452.
(14) Gu, H.; Yang, W.; Seeman, N. C. DNA Scissors Device Used to Measure Muts Binding to DNA Mis-Pairs. *J. Am. Chem. Soc.* **2010**, *132*, 4352−4357.
(15) Ketterer, P.; Willner, E. M.; Dietz, H. Nanoscale Rotary Apparatus Formed from Tight-Fitting 3D DNA Components. *Sci. Adv.* **2016**, *2*, e1501209.
(16) Kuzuya, A.; Sakai, Y.; Yamazaki, T.; Xu, Y.; Komiyama, M. Nanomechanical DNA Origami 'Single-Molecule Beacons' Directly Imaged by Atomic Force Microscopy. *Nat. Commun.* **2011**, *2*, 449.
(17) Kuzyk, A.; Schreiber, R.; Zhang, H.; Govorov, A. O.; Liedl, T.; Liu, N. Reconfigurable 3D Plasmonic Metamolecules. *Nat. Mater.* **2014**, *13*, 862−866.
(18) List, J.; Falgenhauer, E.; Kopperger, E.; Pardatscher, G.; Simmel, F. C. Long-Range Movement of Large Mechanically Interlocked DNA Nanostructures. *Nat. Commun.* **2016**, *7*, 12414.
(19) Marras, A. E.; Zhou, L.; Kolliopoulos, V.; Su, H. J.; Castro, C. E. Directing Folding Pathways for Multi-Component DNA Origami Nanostructures with Complex Topology. *New J. Phys.* **2016**, *18*, 055005.
(20) Marras, A. E.; Zhou, L.; Su, H. J.; Castro, C. E. Programmable Motion of DNA Origami Mechanisms. *Proc. Natl. Acad. Sci. U. S. A.* **2015**, *112*, 713−718.
(21) Mathur, D.; Henderson, E. R. Programmable DNA Nanosystem for Molecular Interrogation. *Sci. Rep.* **2016**, *6*, 27413.
(22) Zhou, L.; Marras, A. E.; Su, H. J.; Castro, C. E. DNA Origami Compliant Nanostructures with Tunable Mechanical Properties. *ACS Nano* **2014**, *8*, 27−34.
(23) Shi, Z.; Castro, C. E.; Arya, G. Conformational Dynamics of Mechanically Compliant DNA Nanostructures from Coarse-Grained Molecular Dynamics Simulations. *ACS Nano* **2017**, *11*, 4617−4630.
(24) Zhou, L.; Marras, A. E.; Su, H. J.; Castro, C. E. Direct Design of an Energy Landscape with Bistable DNA Origami Mechanisms. *Nano Lett.* **2015**, *15*, 1815−1821.
(25) Ke, Y.; Meyer, T.; Shih, W. M.; Bellot, G. Regulation at a Distance of Biomolecular Interactions Using a DNA Origami Nanoactuator. *Nat. Commun.* **2016**, *7*, 10935.
(26) Zadegan, R. M.; Jepsen, M. D.; Thomsen, K. E.; Okholm, A. H.; Schaffert, D. H.; Andersen, E. S.; Birkedal, V.; Kjems, J. Construction of a 4 Zeptoliters Switchable 3D DNA Box Origami. *ACS Nano* **2012**, *6*, 10050−10053.
(27) Douglas, S. M.; Bachelet, I.; Church, G. M. A Logic-Gated Nanorobot for Targeted Transport of Molecular Payloads. *Science* **2012**, *335*, 831−834.
(28) Ranallo, S.; Prevost-Tremblay, C.; Idili, A.; Vallee-Belisle, A.; Ricci, F. Antibody-Powered Nucleic Acid Release Using a DNA-Based Nanomachine. *Nat. Commun.* **2017**, *8*, 15150.
(29) Lavella, G. J.; Jadhav, A. D.; Maharbiz, M. M. A Synthetic Chemomechanical Machine Driven by Ligand-Receptor Bonding. *Nano Lett.* **2012**, *12*, 4983−4987.
(30) Walter, H. K.; Bauer, J.; Steinmeyer, J.; Kuzuya, A.; Niemeyer, C. M.; Wagenknecht, H. A. "DNA Origami Traffic Lights" with a Split Aptamer Sensor for a Bicolor Fluorescence Readout. *Nano Lett.* **2017**, *17*, 2467−2472.
(31) Liu, Z.; Tian, C.; Yu, J.; Li, Y.; Jiang, W.; Mao, C. Self-Assembly of Responsive Multilayered DNA Nanocages. *J. Am. Chem. Soc.* **2015**, *137*, 1730−1733.
(32) Yang, J.; Jiang, S.; Liu, X.; Pan, L.; Zhang, C. Aptamer-Binding Directed DNA Origami Pattern for Logic Gates. *ACS Appl. Mater. Interfaces* **2016**, *8*, 34054−34060.
(33) Bae, W.; Kim, K.; Min, D.; Ryu, J. K.; Hyeon, C.; Yoon, T. Y. Programmed Folding of DNA Origami Structures through Single-Molecule Force Control. *Nat. Commun.* **2014**, *5*, 5654.
(34) Yang, D.; Ward, A.; Halvorsen, K.; Wong, W. P. Multiplexed Single-Molecule Force Spectroscopy Using a Centrifuge. *Nat. Commun.* **2016**, *7*, 11026.
(35) Neuman, K. C.; Nagy, A. Single-Molecule Force Spectroscopy: Optical Tweezers, Magnetic Tweezers and Atomic Force Microscopy. *Nat. Methods* **2008**, *5*, 491−505.
(36) Iwaki, M.; Wickham, S. F.; Ikezaki, K.; Yanagida, T.; Shih, W. M. A Programmable DNA Origami Nanospring That Reveals Force-Induced Adjacent Binding of Myosin Vi Heads. *Nat. Commun.* **2016**, *7*, 13715.
(37) Li, L. H.; Tian, X. J.; Dong, Z. L.; Liu, L. Q.; Tabata, O.; Li, W. J. Manipulation of DNA Origami Nanotubes in Liquid Using Programmable Tapping-Mode Atomic Force Microscopy. *Micro Nano Lett.* **2013**, *8*, 641−645.
(38) Siavashpouri, M.; Wachauf, C. H.; Zakhary, M. J.; Praetorius, F.; Dietz, H.; Dogic, Z. Molecular Engineering of Chiral Colloidal Liquid Crystals Using DNA Origami. *Nat. Mater.* **2017**, *16*, 849−856.
(39) Kopperger, E.; List, J.; Madhira, S.; Rothfischer, F.; Lamb, D. C.; Simmel, F. C. A Self-Assembled Nanoscale Robotic Arm Controlled by Electric Fields. *Science* **2018**, *359*, 296−301.
(40) Lauback, S.; Mattioli, K. R.; Marras, A. E.; Armstrong, M.; Rudibaugh, T. P.; Sooryakumar, R.; Castro, C. E. Real-Time Magnetic Actuation of DNA Nanodevices *Via* Modular Integration with Stiff Micro-Levers. *Nat. Commun.* **2018**, *9*, 1446.
(41) Yang, Y.; Tashiro, R.; Suzuki, Y.; Emura, T.; Hidaka, K.; Sugiyama, H.; Endo, M. A Photoregulated DNA-Based Rotary System and Direct Observation of Its Rotational Movement. *Chem. - Eur. J.* **2017**, *23*, 3979−3985.
(42) Kuzyk, A.; Yang, Y.; Duan, X.; Stoll, S.; Govorov, A. O.; Sugiyama, H.; Endo, M.; Liu, N. A Light-Driven Three-Dimensional Plasmonic Nanosystem That Translates Molecular Motion into Reversible Chiroptical Function. *Nat. Commun.* **2016**, *7*, 10591.
(43) Kuzyk, A.; Urban, M. J.; Idili, A.; Ricci, F.; Liu, N. Selective Control of Reconfigurable Chiral Plasmonic Metamolecules. *Sci. Adv.* **2017**, *3*, e1602803.
(44) SantaLucia, J., Jr. A Unified View of Polymer, Dumbbell, and Oligonucleotide DNA Nearest-Neighbor Thermodynamics. *Proc. Natl. Acad. Sci. U. S. A.* **1998**, *95*, 1460−1465.
(45) Ke, Y.; Douglas, S. M.; Liu, M.; Sharma, J.; Cheng, A.; Leung, A.; Liu, Y.; Shih, W. M.; Yan, H. Multilayer DNA Origami Packed on a Square Lattice. *J. Am. Chem. Soc.* **2009**, *131*, 15903−15908.
(46) Martin, T. G.; Dietz, H. Magnesium-Free Self-Assembly of Multi-Layer DNA Objects. *Nat. Commun.* **2012**, *3*, 1103.
(47) Douglas, S. M.; Dietz, H.; Liedl, T.; Hogberg, B.; Graf, F.; Shih, W. M. Self-Assembly of DNA into Nanoscale Three-Dimensional Shapes. *Nature* **2009**, *459*, 414−418.
(48) Markham, N. R.; Zuker, M., UNAFold. In *Bioinformatics*; Keith, J. M., Ed.; Humana Press: New York, 2008; pp 3−31.
(49) Markham, N. R.; Zuker, M. DINAMelt Web Server for Nucleic Acid Melting Prediction. *Nucleic Acids Res.* **2005**, *33*, W577−581.
(50) Tomov, T. E.; Tsukanov, R.; Glick, Y.; Berger, Y.; Liber, M.; Avrahami, D.; Gerber, D.; Nir, E. DNA Bipedal Motor Achieves a Large Number of Steps Due to Operation Using Microfluidics-Based Interface. *ACS Nano* **2017**, *11*, 4002−4008.
(51) Northcutt, R. G.; Sundaresan, V. B. Phospholipid Vesicles as Soft Templates for Electropolymerization of Nanostructured Polypyrrole Membranes with Long Range Order. *J. Mater. Chem. A* **2014**, *2*, 11784−11791.
(52) Douglas, S. M.; Marblestone, A. H.; Teerapittayanon, S.; Vazquez, A.; Church, G. M.; Shih, W. M. Rapid Prototyping of 3D DNA-Origami Shapes with caDNAno. *Nucleic Acids Res.* **2009**, *37*, 5001−5006.

DOI: 10.1021/acsnano.8b04817
ACS Nano 2018, 12, 9484−9494

(53) Castro, C. E.; Kilchherr, F.; Kim, D. N.; Shiao, E. L.; Wauer, T.; Wortmann, P.; Bathe, M.; Dietz, H. A Primer to Scaffolded DNA Origami. *Nat. Methods* **2011**, *8*, 221−229.
(54) Stahl, E.; Martin, T. G.; Praetorius, F.; Dietz, H. Facile and Scalable Preparation of Pure and Dense DNA Origami Solutions. *Angew. Chem., Int. Ed.* **2014**, *53*, 12735−12740.
(55) Kubo, R. *Thermodynamics: An Advanced Course with Problems and Solutions*; North-Holland: Amsterdam, The Netherlands, 1968; Vol. *1*.

DOI: 10.1021/acsnano.8b04817
ACS Nano 2018, 12, 9484−9494